Fully Developed Viscous Flow in Coiled Circular Pipes

The Navier-Stokes equations in stream-function/vorticity form were solved numerically by over-relaxation for the case of steady state, fully developed, isothermal, incompressible viscous Newtonian flow within a rigorously treated toroidal geometry. Solutions were obtained for curvature ratios ranging from 5 to 100 and for Dean numbers as low as 1 and as high as 1000. The Dean number was demonstrated to be the principal parameter to characterize toroidal flow; however, a second-order dependence upon the curvature ratio above that expressed in the Dean number was observed. Comparisons of the numerically computed axial-velocity profiles were made with experimental data. The cross-sectional pressure distribution was calculated, and a correlation is presented for a diametral pressure drop in terms of the Dean number.

LARRY R. AUSTIN and J. D. SEADER

Department of Chemical Engineering
The University of Utah
Salt Lake City, Utah 84112

SCOPE

Straight circular tubes have found widespread use in operations involving fluid dynamics, heat transfer, mass transfer, and chemical-reaction kinetics. For laminar flow, a large number of analytical investigations and supporting experimental studies have been reported that permit, in many cases, quite accurate predictions of transport phenomena, including transport with simultaneous chemical reaction.

Curved configurations of circular tubes—such as partial coils, single coils, helical coils, and spiral coils—have received far less attention in the literature despite their frequent use in heat exchangers, chemical reactors, rocket engines, and other apparatus, equipment, or devices. In some cases, the use of curved tubes is necessitated because of geometrical restrictions. However, it is also becoming increasingly apparent that the nature of the complex primary (axial direction) and secondary (normal to primary) flow patterns in curved tubes makes possible some definite advantages of this configuration over straight tubes for a number of situations. In fully developed curved-tube viscous flow, the primary-flow-velocity profile is distorted from its parabolic straight-tube-flow counterpart, a secondary flow is established that consists of two vortices, and the resultant combined primary and secondary flow patterns cause a fluid element to have a screw-like motion. At one instant, a fluid element may be traveling near the very center of the tube cross section. After a short period of time and a short axial distance downstream, the same fluid element may be found very near the outside wall of the tube. The nature of curved-tube viscous-fluid motion, as compared with simple straight-tube parabolic flow, causes a higher axial-pressure gradient, a higher critical Reynolds number for transition to turbulent flow, a diametral-pressure gradient, a fluid-element residence-time distribution that more closely approximates plug flow, relatively high average heat-transfer and mass-transfer rates per unit axial pressure drop, especially for high-Prandtl-number and high-Schmidt-number fluids, and significant peripheral distributions of the transport rates. The latter effect can be utilized to advantage in applications where the peripheral boundary conditions are asymmetrical.

Of fundamental interest to the development of a complete understanding of viscous-flow phenomena in curved or coiled tubes is the nature of the velocity and pressure distributions in the fully-developed flow region. In studies by previous investigators, these profiles have been found to depend strongly on the Dean number N_{De} where $N_{De} = N_{Re}(R/R_c)^{1/2}$, R is the pipe inside radius, and R_c is the coil radius of curvature. At low Dean numbers, open-form analytical solutions have been achieved; numerical methods have been successful to moderate Dean numbers of approximately 300; and an approximate combined boundary-layer/potential-flow core theory has been applied at high Dean numbers. The objective of this study was to develop a rapidly converging and reasonably accurate numerical solution to the equations of fluid motion so that velocity and pressure profiles could be computed over a much wider range of Dean numbers and curvature ratios R_c/R than previously.

CONCLUSIONS AND SIGNIFICANCE

Solutions of the equations of fluid motion were achieved for the case of steady state, fully-developed, isothermal, incompressible, viscous Newtonian flow within a toroidal-type coiled-tube geometry. Thus, the effect of coil pitch was not investigated. The computations covered a Dean-number range of 1 to 1000, a Reynolds-number range of 10 to 4000, and a curvature-ratio range of 5 to 100. The numerical mathematical technique that was employed involved the expression of the equations of motion in terms of the axial-velocity component, the stream function of the secondary flow, and the axial component of the vorticity. The resulting partial-differential equations were ex-

Correspondence concerning this paper should be addressed to J. D. Seader. L. R. Austin is now with E. I. du Pont de Nemours and Company, Chattanooga, Tennessee.

pressed as finite-difference equations by the use of first central-difference operators and then solved by a sequential application of a successive over-relaxation technique. Several methods were used to check convergence.

As shown in Figure 4, the low-Dean number secondary-flow streamlines are essentially symmetrical and in agreement with the previous analytical solution of Dean, the pioneering theoretician for curved-tube viscous flow. The secondary flow is directed outward (with respect to the coil axis) along a path near the pipe diameter and then back along a path near the pipe wall. As the Dean number is increased, causing an intensification of the secondary flow, nonconvex regions are developed by the formation of dimples in the streamlines of the secondary flow. These streamlines depart from their symmetrical nature in the half plane, and the vortex center shifts toward the wall and toward the axis of the coil. As shown in Figure 4, at a Dean number of approximately 400, little difference can be distinguished in the secondary-flow streamlines over a wide range of curvature ratio. Thus, the effect of the curvature ratio is accounted for mainly in the Dean number. The secondary-flow streamlines for the approximate combined boundary-layer/potential-flow core theory at a Dean number of 400, as shown in Figure 5, differ significantly from the numerical solution.

At low Dean numbers where the secondary flow is small, the axial-velocity profile is essentially parabolic and unaltered from straight-tube laminar flow. As shown in Figure 6 for a Dean number of approximately 400, the maximum velocity at the diameter of full-circle symmetry and that for four adjacent parallel chords spanning the half-circle cross section are skewed. For the same conditions of Dean number and curvature ratio, Figure 7 shows that the central portion of the velocity surface is somewhat dished in the direction parallel to the axis of the coil. This dished effect becomes slightly more pronounced at higher Dean numbers. The numerically computed profiles were in excellent agreement with experimental data.

Pressure distributions for the same locations in the secondary-flow plane as those in Figure 6 are shown in Figure 8. In general, the pressure distribution is dependent mainly on the Dean number; and the pressure increases smoothly from the inside to the outside of the pipe with respect to the coil axis. The computed dimensionless diametral-pressure-drop data are correlated in Figure 9 and are in reasonably close proximity to the plot of Lansford's equation (1935), which was determined under the assumption of an ideal, uniform, primary-flow velocity distribution. As shown in Table 2, at moderate-to-high Dean numbers, the dimensionless average diametral-pressure gradient in the secondary-flow plane is greater than the negative axial-pressure gradient.

The axial-pressure gradient for curved-tube flow is generally correlated in terms of a friction factor that is normalized with respect to the straight-tube-flow friction factor for the same Reynolds number. The computed results shown in Figure 10 are well grouped around White's experimental correlation and exhibit a slight dependence on the curvature ratio, as predicted previously by Topakoglu (1967), at low Dean numbers.

The results presented here or calculated at other conditions by the computer program cited can be utilized to compute pressure drops, residence-time distributions, and heat- and/or mass-transfer rates (both axial and peripheral variations). In an extension of the work presented here, Kalb and Seader (1972) have utilized the velocity profiles to compute heat transfer to steady viscous flow in a toroid for fully developed velocity and temperature fields under the thermal boundary condition of axially uniform wall heat flux with peripherally uniform wall temperature for Dean numbers from 1 to 1,200 and Prandtl numbers from 0.005 to 1,600. Order-of-magnitude increases in the average heat-transfer coefficient for curved tube flow over that for straight-tube flow are predicted, particularly at high Dean numbers and for high Prandtl number fluids.

Fluid flow within helically coiled tubes is common in many industrial operations, particularly those involving heat transfer. Toroidal flow is the limiting case of helical flow with zero pitch. The mode of fluid flow in coils is characterized by a secondary flow field, which is superimposed upon the axial-velocity flow field. The secondary flow field divides itself along the diameter of the toroid into two mirror images. Flow is directed outward along the diameter, which then returns to the center by following the tube wall. This secondary-flow action causes the diametral axial-velocity profile to be skewed toward the outside of the coil. Not only are velocity profiles altered as compared to straight-pipe flow, but also the axial-pressure drop is increased and a diametral pressure difference is established. Fundamental information on velocity and pressure profiles is useful in establishing heat- and mass-transfer rates and homogeneous chemical-kinetic phenomena for flow in curved tubes.

Active experimental work with helical-flow systems dates back to the beginning of the twentieth century. Considerable experimental work has been done by Grindley (1908), Eustice (1910), White (1929), Keulegan and Beij (1937), Seban and McLaughlin (1963), Kubair and Kuloor (1963), Schmidt (1967), Ito (1969), and Larrain and Bonilla (1970) to establish a pressure-drop relationship. The first reliable resistance law was determined by White (1929). His law has been verified many times since. He introduced a dimensionless parameter, now known as the Dean number, which has proved to be the most important single parameter with which helical flow can be characterized. Dye-injection experiments, performed first by Eustice (1911), and later by Taylor (1929), were fundamental in demonstrating the secondary flow, which is characteristic of all helical flow. Taylor's experiments also showed that, depending on the ratio of the radius of curvature to the tube radius (curvature ratio), the critical Reynolds number was increased to values beyond the value of 2,100 usually accepted for straight-tube flow. For example, at a curvature ratio of 18.7, a critical Reynolds number of 5830 was observed.

Several theoretical attempts have been made by Dean (1927, 1928), Topakoglu (1967), McConalogue and Srivastava (1968), Truesdell and Adler (1970), Larrain and Bonilla (1970), and Akiyama and Cheng (1971) to solve the equations of fluid motion for the case of toroidal flow. The first classical work is attributed to Dean (1927, 1928). His original solution was valid for creeping flow only ($N_{De} < 1$) and failed to show any increased flow resistance over straight-pipe flow but did predict the form of the secondary-flow field, as previously observed by Eustice (1911) in his dye-injection experiments. Truesdell and Adler (1970) produced a numerical solution that was

completely rigorous for a toroidal system; however, their method of solution proved to be unstable at Dean numbers much larger than 200. The work described here is an outgrowth of the work by Truesdell and Adler. Basic differences, as discussed in detail by Austin (1971), are:

1. A toroidal coordinate system is used here, while Truesdell and Adler employed a rectangular coordinate system.
2. The solution algorithm in this work is based on the vorticity field, while Truesdell and Adler solved a fourth-order partial differential equation in terms of the stream function.

Akiyama and Cheng (1971) also utilized the vorticity concept but restricted their solution to very large curvature ratios and could not obtain solutions beyond a Dean number of 300.

THE EQUATIONS OF FLUID MOTION

A vector representation of the steady state, constant-property Navier-Stokes equation can be expressed (Bird et al., 1960) as

$$\tfrac{1}{2}\nabla(v\cdot v) - v\times(\nabla\times v) = -\frac{1}{\rho}\nabla p + \nu\nabla^2 v, \quad (1)$$

This equation may be rendered dimensionless by introducing the following dimensionless variables, where R is a characteristic length:

$$V = \frac{R\,v}{\nu} \quad (2)$$

$$P = \frac{R^2\,p}{\rho\,\nu^2} \quad (3)$$

and by replacing the customary dimensional-vector differential operator ∇ with a dimensionless form $R\nabla$. The resulting dimensionless equivalent of Equation (1) is

$$\tfrac{1}{2}\nabla(V\cdot V) - V\times(\nabla\times V) = -\nabla P + \nabla^2 V. \quad (4)$$

It is convenient to introduce the vorticity ω as discussed by Brodkey (1967), into Equation (4), where

$$\omega = \nabla\times V. \quad (5)$$

Accordingly, an alternate form of Equation (4) is

$$\tfrac{1}{2}\nabla(V\cdot V) - V\times\omega = -\nabla P - \nabla\times\omega. \quad (6)$$

Equation (6) was solved numerically in terms of a toroidal geometry, that is, with the assumption that the coil has no pitch. The pitch effect might become important as the radius of curvature for the coil approaches the radius of the coil tube. The toroidal coordinate system is shown in Figure 1 where the position variables are ψ, θ, and r. A radius-of-curvature parameter R_c is also required to complete the geometric specification. Here, both r and R_c are understood to be normalized with respect to the characteristic length R which was chosen to be the tube radius. Equation (6) was applied to this toroidal coordinate system by means of dimensionless scale factors, which are readily shown by Austin (1971) to be

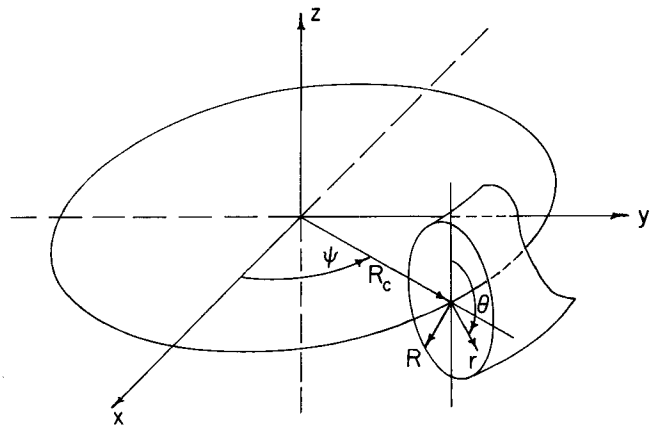

Fig. 1. The toroidal geometry.

$$h_\psi = R_c + r\sin\theta \quad (7)$$

$$h_r = 1.0 \quad (8)$$

and

$$h_\theta = r \quad (9)$$

Fully developed flow was assumed.

By expanding Equation (6) into its three components, then differentiating the r and θ components with regard to θ and r, respectively, and combining the resulting expressions, the unknown pressure is eliminated. The unknowns ω_r and ω_θ are eliminated by introducing V_ψ through its relationship to the definition of vorticity in Equation (5)

$$\omega_r = \frac{1}{r\,h_\psi}\left[\frac{\partial}{\partial\theta}(h_\psi V_\psi)\right] \quad (10)$$

and

$$\omega_\theta = -\frac{1}{h_\psi}\left[\frac{\partial}{\partial r}(h_\psi V_\psi)\right] \quad (11)$$

The ω_ψ component of Equation (5) is retained.

The unknowns V_r and V_θ may be eliminated by introducing the definition of a stream function for the secondary flow in the cross section such that the equation of continuity for the fully developed toroidal flow is satisfied. These defining equations are

$$V_r = -\frac{1}{r\,h_\psi}\frac{\partial S}{\partial\theta} \quad (12)$$

and

$$V_\theta = \frac{1}{h_\psi}\frac{\partial S}{\partial r} \quad (13)$$

The final result is three elliptic second-order partial differential equations in three dependent variables—ω_ψ, V_ψ, and S—and two parameters—R_c and $\partial P/\partial\psi$—namely:

1. The defining equation for the axial component of the vorticity

$$\omega_\psi = \left[\frac{1}{r\,h_\psi} - \frac{\sin\theta}{h_\psi^2}\right]\frac{\partial S}{\partial r} + \frac{1}{h_\psi}\frac{\partial^2 S}{\partial r^2} - \frac{\cos\theta}{r\,h_\psi^2}\frac{\partial S}{\partial\theta} + \frac{1}{r^2\,h_\psi}\frac{\partial^2 S}{\partial\theta^2} \quad (14)$$

2. The axial component of the Navier-Stokes equation

$$A_\psi V_\psi + B\frac{\partial V_\psi}{\partial\theta} + C\frac{\partial V_\psi}{\partial r} - \frac{\partial^2 V_\psi}{\partial r^2} - \frac{1}{r^2}\frac{\partial^2 V_\psi}{\partial\theta^2} = -\frac{1}{h_\psi}\frac{\partial P}{\partial\psi} \quad (15)$$

where

$$A_\psi = \frac{1}{h_\psi^2}\left[1 + \cos\theta\frac{\partial S}{\partial r} - \frac{\sin\theta}{r}\frac{\partial S}{\partial\theta}\right] \quad (16)$$

$$B = \frac{1}{r\,h_\psi}\left[\frac{\partial S}{\partial r} - \cos\theta\right] \quad (17)$$

and

$$C = -\left[\frac{1}{r} + \frac{\sin\theta}{h_\psi} + \frac{1}{r\,h_\psi}\frac{\partial S}{\partial\theta}\right] \tag{18}$$

3. The combined equations for the r and θ components of the Navier-Stokes equation

$$A_\omega\,\omega_\psi + B\frac{\partial\omega_\psi}{\partial\theta} + C\frac{\partial\omega_\psi}{\partial r} - \frac{\partial^2\omega_\psi}{\partial r^2} - \frac{1}{r^2}\frac{\partial^2\omega_\psi}{\partial\theta^2} = D_\omega \tag{19}$$

where

$$A_\omega = \frac{1}{h_\psi^2}\left[1 - \cos\theta\frac{\partial S}{\partial r} + \frac{\sin\theta}{r}\frac{\partial S}{\partial\theta}\right] \tag{20}$$

and

$$D_\omega = \frac{2V_\psi}{h_\psi}\left[\cos\theta\frac{\partial V_\psi}{\partial r} - \frac{\sin\theta}{r}\frac{\partial V_\psi}{\partial\theta}\right] \tag{21}$$

Although Equations (15) and (19) are nonlinear, the iterative-solution procedure described below involved linearized forms of these equations, wherein the dependent-variable terms in the defining relationships for A_ψ, A_ω, B, C, and D_ω were based on the solution of previously calculated values.

BOUNDARY CONDITIONS

Because of the symmetry of the flow field, only one half of the cross-sectional region required consideration. The regional boundary was divided into four distinct sections which are shown in Figure 2 where I and J are radial and peripheral grid-point locations, respectively, that were used in the numerical calculations described later. These sections are

1. The curved portion of the outer wall ($I = 1$, $1 \leq J \leq 21$)
2. The inside half of the diameter ($1 \leq I \leq 20$, $J = 1$)
3. The outside half of the diameter ($1 \leq I \leq 20$, $J = 21$)
4. The singular point ($I = 21$, $1 \leq J \leq 21$).

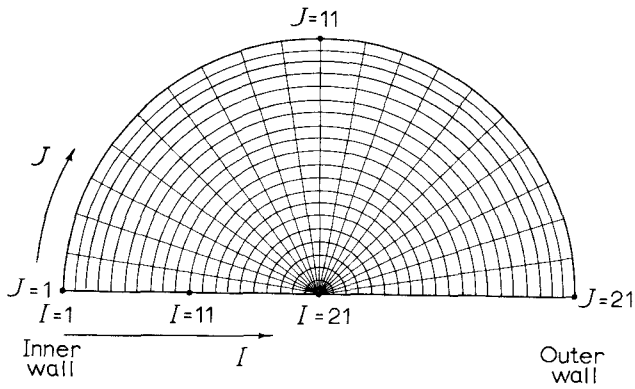

Fig. 2. The computational grid region.

TABLE 1. BOUNDARY CONDITIONS FOR THE THREE VARIABLES

Variable	Section 1	Section 2	Section 3	Section 4
V_ψ	0	$\frac{\partial V_\psi}{\partial\theta} = 0$	$\frac{\partial V_\psi}{\partial\theta} = 0$	$\frac{\partial V_\psi}{\partial r}\Big\|_{\theta=0} = 0$
S	0	0	0	0
ω_ψ	$\frac{1}{h_\psi}\frac{\partial^2 S}{\partial r^2} = \omega_\psi$	0	0	0

The boundary conditions were deduced in a logical manner from the equations of motion by Austin (1971), based on two main assumptions:

1. That the no-slip condition exists at solid boundaries, that is, the velocity at the wall is zero, and
2. That a symmetrical condition exists across the central diameter.

The resulting boundary conditions for each of the four boundary sections are summarized in Table 1.

FINITE-DIFFERENCE EQUATIONS

Each of the governing relationships given by Equations (14), (15), and (19) were expressed as finite-difference equations by use of first central-difference operators. As described by Austin (1971), special one-sided operators after the method of Vrentas et al. (1966) were used at the pipe wall to improve solution stability. Corresponding terms were then combined such that each equation could be expressed as coefficients multiplied by the dependent variable at the mesh point in question and its four nearest neighbors. These equations, in the computational molecule form of Lapidus (1962), are

1. The axial component of the vorticity

$$\begin{bmatrix} & Z_1 & \\ Z_2 & Z_3 & Z_4 \\ & Z_5 & \end{bmatrix} S = r^2(\Delta r)h_\psi\,\omega_\psi \tag{22}$$

where

$$Z_1 = r^2\left[\frac{1}{2r} + \frac{1}{\Delta r} - \frac{\sin\theta}{2h_\psi}\right]$$

$$Z_2 = \frac{\Delta r}{\Delta\theta}\left[\frac{r\cos\theta}{2h_\psi} + \frac{1}{\Delta\theta}\right]$$

$$Z_3 = -2\left[\frac{r^2}{\Delta r} + \frac{\Delta r}{(\Delta\theta)^2}\right]$$

$$Z_4 = \frac{\Delta r}{\Delta\theta}\left[-\frac{r\cos\theta}{2h_\psi} + \frac{1}{\Delta\theta}\right]$$

and

$$Z_5 = r^2\left[-\frac{1}{2r} + \frac{1}{\Delta r} + \frac{\sin\theta}{2h_\psi}\right]$$

2. The axial component of the Navier-Stokes equation

$$\begin{bmatrix} & X_1 & \\ X_2 & X_3 & X_4 \\ & X_5 & \end{bmatrix} V_\psi = -\frac{r^2}{h_\psi}\frac{\partial P}{\partial\psi} \tag{23}$$

where

$$X_1 = \frac{r^2 C}{2\Delta r} - \frac{r^2}{(\Delta r)^2}$$

$$X_2 = -\frac{r^2 B}{2\Delta\theta} - \frac{1}{(\Delta\theta)^2}$$

$$X_3 = r^2\,A_\psi + \frac{2r^2}{(\Delta r)^2} + \frac{2}{(\Delta\theta)^2}$$

$$X_4 = \frac{r^2 B}{2\Delta\theta} - \frac{1}{(\Delta\theta)^2}$$

and

$$X_5 = -\frac{r^2 C}{2\Delta r} - \frac{r^2}{(\Delta r)^2}$$

3. The combined r and θ components of the Navier-Stokes equation

$$\begin{bmatrix} & Y_1 & \\ Y_2 & Y_3 & Y_4 \\ & Y_5 & \end{bmatrix} \omega_\psi = r^2 D_\omega \qquad (24)$$

where

$$Y_k = X_k$$

$$k = 1, 2, 4, 5,$$

and

$$Y_3 = r^2 A_\omega + \frac{2r^2}{(\Delta r)^2} + \frac{2}{(\Delta\theta)^2}$$

The above three finite-difference equations were solved by a standard successive over-relaxation technique, as described by Greenspan (1965). The order in which the equations were solved was critical for stable convergence and is discussed next.

COMPUTATIONAL ALGORITHM

A flow diagram of the major calculational steps involved in solving the governing equations appears as Figure 3. The starting data included boundary conditions as well as the assumed initial values of the three dependent variables at all other grid points. In general, in computations for a particular curvature ratio and axial-pressure gradient corresponding to a certain Dean number, the assumed initial values were set equal to the final results obtained from computations for the next lowest Dean number. The first case, for a low axial-pressure gradient corresponding to a Dean number of approximately one, was initiated under the assumption of straight-pipe values; that is, $S = \omega_\psi = 0$ and V_ψ based on a parabolic profile.

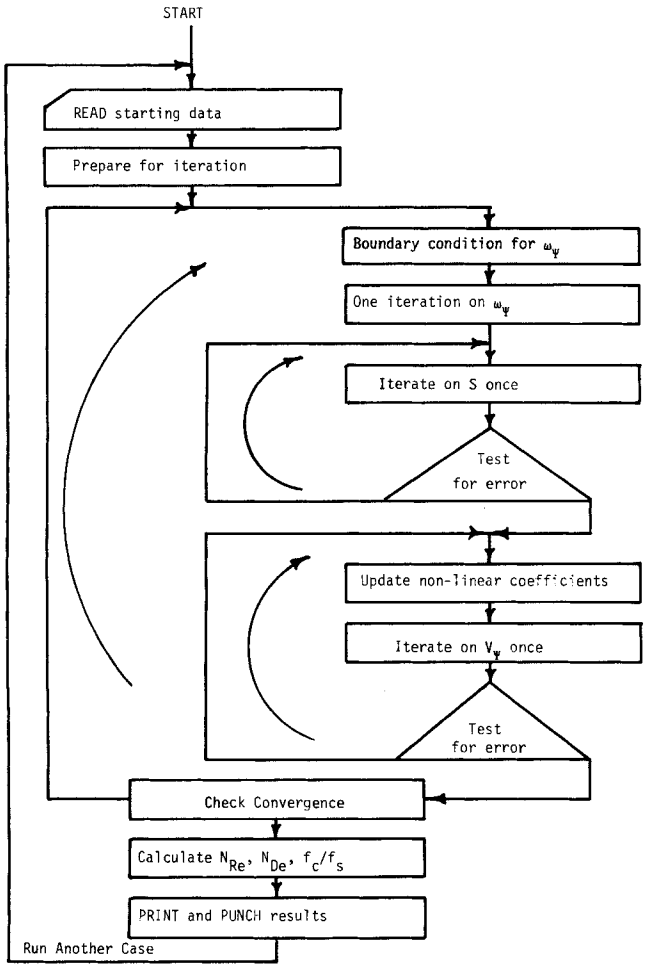

Fig. 3. Flow chart for computer program.

As shown in Figure 3, the method of solution was, first, to iterate Equation (24) one time, updating the vorticity at each interior point, then to solve Equation (22) for the stream function. Normally, this equation was iterated a number of times (5 to 15) to obtain a rather smooth solution surface, which greatly facilitated computational stability since the boundary condition for the vorticity depends upon the derivative of the stream function. Next, Equation (23) was solved for the axial component of the velocity; this nonlinear equation was also iterated to accelerate overall convergence. These three steps constituted one complete major iteration.

Generally, a number of major iterations were performed in order to obtain a converged solution. As discussed in more detail below, satisfactory convergence of the solution was tested by comparing successive results as the spatial grid size was reduced, comparing friction factors computed for a given run by two alternate expressions, and comparing the numerical results with experimental data.

The spatial-convergence check was performed by obtaining solutions with an 11 × 11 grid-point mesh and a 21 × 21 grid-point mesh for Dean numbers as high as 400. Agreement between the two results was excellent. As a further check on spatial convergence, dimensionless secondary velocities at the singular point $I = 21$ were computed for all values of the peripheral grid-point location J. Excellent agreement among the values was obtained. For example, at a Dean number of 603 and a curvature ratio of 9.06, the 21 values covered a very narrow range of only 21.88 to 21.90.

In practice, it was found possible to obtain a satisfactorily converged solution by terminating a run when successive values of the three dependent variables obtained during major iterations changed by less than 0.001%. This normally required on the order of 100 major iterations. Convergence was aided by proper selection of relaxation factors that were assigned in the manner of Greenspan (1965). The best relaxation factor for the stream function was one. This is in agreement with Akiyama and Cheng (1971). Factors for the vorticity and axial velocity were required to decrease from one with increasing Dean number. Once a completely converged solution was obtained, values of the Reynolds number, the Dean number, and the friction factor were computed.

RESULTS AND DISCUSSION

As discussed above, the three variables actually obtained from the previously described numerical computations were the axial component of the vorticity, the stream function, and the axial component of the velocity. Primitive variables were computed numerically as follows: The radial and angular components of the secondary velocity were obtained by solution of Equations (12) and (13), respectively, with fourth-order difference operators. The pressure distribution for the cross section was calculated by integration of the radial component of Equation (6), starting with a reference value of zero for the pressure at

* A listing of the Fortran computer program has been deposited as Document No. 01994 with the National Auxiliary Publications Service (NAPS), c/o Microfiche Publications, 305 East 46 Street, New York 10017 and may be obtained for $2.00 for microfiche or $5.00 for photocopies.

Table 2. Run Conditions for Numerical Calculations

Run	$\partial P/\partial \psi$	R_c	N_{Re}	N_{De}	f_c/f_s	$-\Delta P_D/\Delta P_\psi$
1	−4,000	100.0	9.999	0.999	1.000	0.0105
2	−20,000	100.0	49.98	4.998	1.001	0.053
3	−50,000	100.0	123.9	12.39	1.009	0.1295
4	−90,000	100.0	213.6	21.36	1.053	0.215
5	−600,000	100.0	1,003.0	100.3	1.495	0.595
6	−1,020,000	100.0	1,499.0	149.9	1.701	0.765
7	−1,510,000	100.0	2,001.0	200.1	1.886	0.91
8	−2,650,000	100.0	2,997.0	299.7	2.210	1.14
9	−4,000,000	100.0	4,018.0	401.8	2.489	1.325
10	−421,000	29.1	1,620.0	300.4	2.232	2.065
11	−570,000	29.1	2,014.0	373.4	2.431	—
12	−148,000	14.4	1,138.0	300.0	2.257	2.835
13	−75,000	9.06	904.4	300.5	2.288	3.45
14	−201,000	9.06	1,816.0	603.3	3.054	5.425
15	−309,000	9.06	2,437.0	809.6	3.499	5.765
16	−321,000	9.06	2,500.0	830.6	3.543	—
17	−430,000	9.06	3,034.0	1,008.0	3.911	6.5
18	−50,300	6.94	786.0	298.4	2.305	3.825
19	−200	5.0	9.980	4.463	1.002	0.219
20	−450	5.0	22.17	9.917	1.015	0.465
21	−950	5.0	44.19	19.76	1.075	0.845
22	−18,000	5.0	448.7	200.7	2.006	3.50
23	−31,500	5.0	670.6	299.9	2.349	4.33
24	−47,400	5.0	897.3	401.3	2.641	5.05
25*	−1,910,000	40.0	3,956.7	625.6	3.017	—

* Close to the conditions for the experimental velocity profile reported by Mori and Nakayama (1965) in Figure 14 of their article.

the center point.

A total of 25 computational cases were run on a Univac 1108 digital computer. The run conditions and computed parameters are listed in Table 2. Curvature ratios were varied from 5 to 100, and specified dimensionless axial-pressure gradients resulted in a Dean-number range of approximately 1 to 1000 and a Reynolds-number range of approximately 10 to 4000. Runs at conditions other than those listed in Table 2, for Dean numbers as high as 1000, can be made rapidly with the aforementioned computer program.* Although runs for Dean numbers greater than 500 are shown for a curvature ratio of 9.06 only, calculations at other curvature ratios can be made with the computer program.

Velocity Profiles

The velocity distribution in the secondary-flow plane is best displayed by means of the stream function. Lines of constant stream-function values represent the projected secondary-motion streamlines that are superimposed on the axial-velocity flow field. Typical contours of this function are shown in Figure 4 for several conditions. At a Dean number of 1.0 and a curvature ratio of 100, the streamline curves bound convex regions that are essentially symmetrical about a radius at $\theta = 0°$ in the half circle. The center of the secondary vortex lies somewhat closer to the diameter of full-circle symmetry than to the upper wall. The low-Dean-number streamlines are in agreement with the analytical solution obtained by Dean (1927). However, as the Dean number is increased causing an intensification of the secondary flow, nonconvex regions are developed by the formation of dimples in the streamlines, which also depart from their symmetrical nature in the half plane. In addition, the vortex center shifts toward the upper wall and toward the axis of the toroid. Such alterations in the nature of the streamlines are noticeable above Dean numbers of approximately 100, as observed by Truesdell and

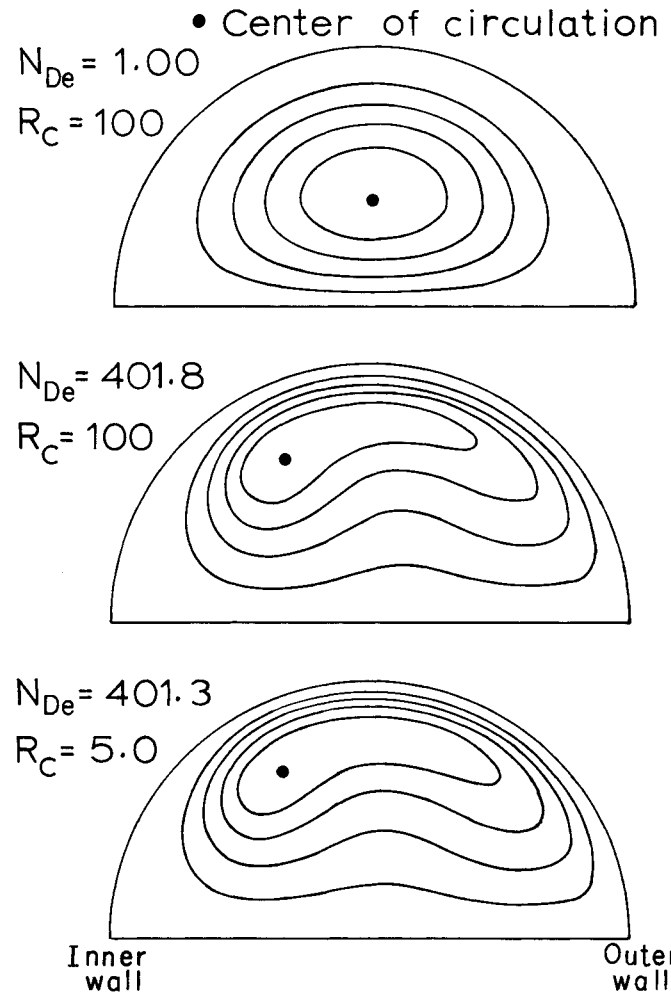

Fig. 4. Computed stream-function contours.

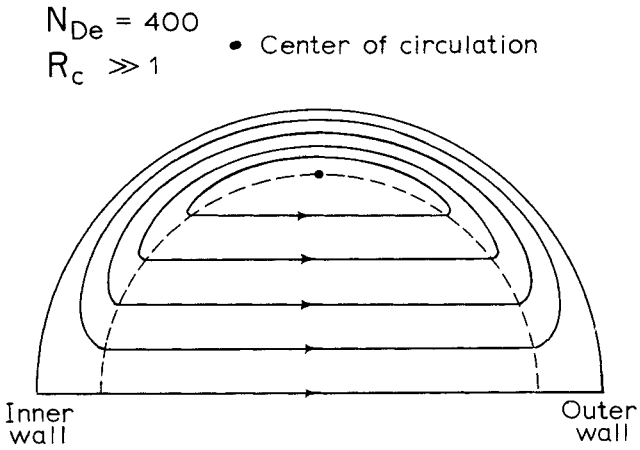

Fig. 5. Stream-function contour for boundary-layer, potential-flow model.

Adler (1970). Truesdell (1963) shows the secondary-flow pattern for a Dean number of 122.9 and a curvature ratio of 100. Secondary-flow patterns similar to those of Figure 4 are shown by Akiyama and Cheng (1971) for very large curvature ratios. Figure 4 includes the results of our computations for a Dean number of 401.8 and a curvature ratio of 100. If this Dean number is held essentially constant while the curvature ratio is reduced drastically to a value of 5.0, the nature of the secondary flow is altered only slightly, as can be observed in Figure 4. Thus the effect of the curvature ratio is accounted for mainly in the Dean number, but it does have an additional, although slight, effect on the secondary flow.

Results of the application of the approximate boundary-layer, potential-flow model of Mori and Nakayama (1965) to the calculation of streamlines for a Dean number of 400 and a large curvature ratio are shown in Figure 5. Their assumption of uniform secondary flow outward in the central-core region and their calculation of the location of the center of the secondary-flow circulation are seen to differ significantly from the results of the numerical solution, shown in Figure 4 for the same Dean number. This difference was very marked below a Dean number of 200.

At a Dean number of 1.0, the axial-velocity profile for $R_c = 100$ is essentially parabolic and unaltered from fully developed, straight-pipe laminar flow. However, at Dean numbers greater than approximately 10, the maximum velocity at the diameter of full-circle symmetry tends to shift outward, away from the axis of the toroid.* Dimensionless axial-velocity [see Equation (2)] profiles for the diameter of full-circle symmetry, as well as for four adjacent parallel chords spanning the half-circle cross section, are shown in Figure 6 for a Dean number of 401.3 and a curvature ratio of 5.0. The entire axial-velocity surface for the same conditions is depicted in Figure 7. The central portion of the velocity surface is somewhat dished in the direction parallel to the axis of the toroid. This dished effect becomes slightly more pronounced at higher Dean numbers.

Comparisons of the numerically computed axial-velocity profiles were made with experimental data obtained by Austin (1971) with air flow at Dean numbers of 372 and 832 for curvature ratios of 29.1 and 9.06, respectively. The agreement was excellent, with the small deviations believed to be due to a combination of factors, including experimental error, a pipe-coil cross section that was slightly flattened during bending to form the coil, and the coil pitch.

A comparison was also made with the experimental axial-velocity-profile data of Mori and Nakayama (1965) for a Reynolds number of 4000, a curvature ratio of 40, and a corresponding Dean number of 632.5. This is included as Run 25 in Table 2. The agreement was excellent for the velocity profile in the horizontal plane. For the vertical plane, the data of Mori and Nakayama scattered somewhat. Our numerical results for the vertical plane were within their data scatter.

Pressure Distribution in the Secondary-flow Plane

A typical plot of the dimensionless pressure [see Equation (3)] distribution in the secondary-flow plane for the diameter of full-circle symmetry, as well as for four ad-

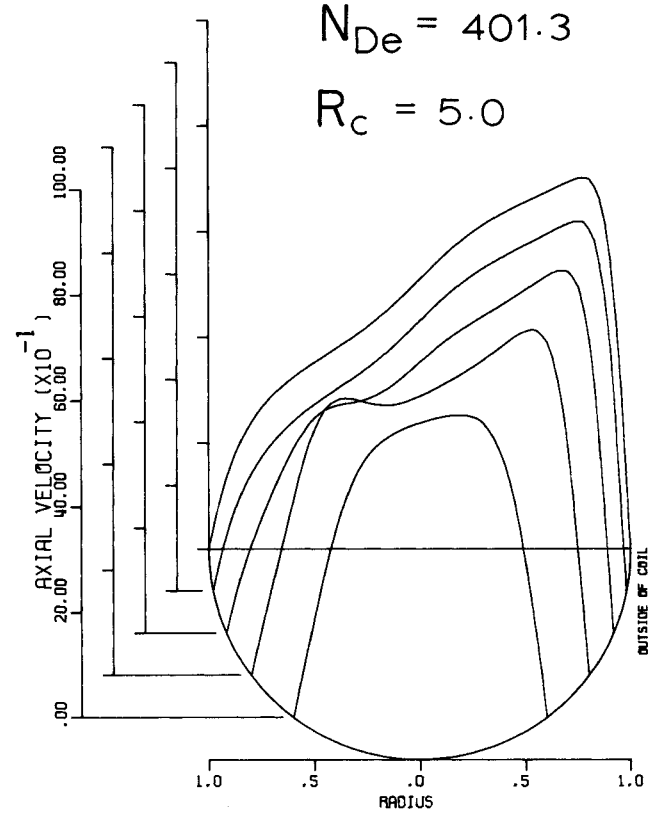

Fig. 6. Axial-velocity profiles.

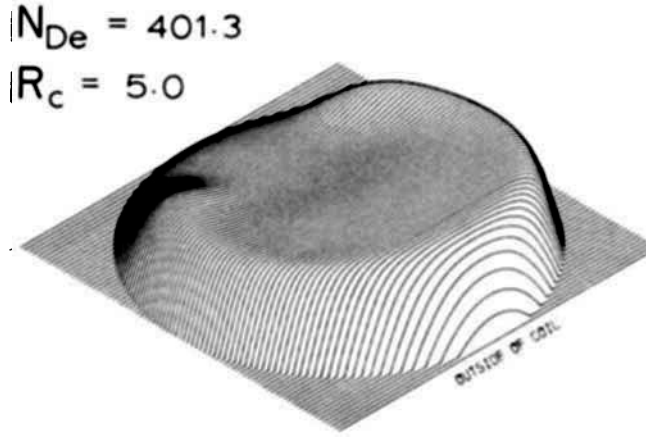

Fig. 7. Axial-velocity surface.

* Lorrain and Bonilla (1970) show that, for very low Dean numbers and low curvature ratios, the maximum velocity can occur slightly closer to the inner wall of the pipe. This effect was observed also in the numerical results of this study.

jacent parallel chords spanning the half-circle cross section, is shown in Figure 8 for a Dean number of 401.3 and a curvature ratio of 5.0. In general, the pressure increases smoothly from the inside to the outside of the toroid with respect to the axis of the toroid. The secondary pressure distribution was dependent mainly on the Dean number and only slightly on the curvature ratio as an additional independent parameter. Of particular interest is the dimensionless diametral pressure difference,* which is correlated empirically with the Dean number, as shown in Figure 9. An approximate solution for the diametral pressure drop was obtained by Lansford (1935) by making a force balance with the assumption of an ideal, uniform, primary-flow velocity distribution. The dimensionless form of Lansford's resulting equation is $\Delta P_D = (N_{De})^2/2$. As shown in Figure 9, this equation is in reasonably good agreement with the computed points. The experimental data of Kubair and Kuloor (1963) and Tsuji and Kawashima as shown by Ito (1969) were found to be in excellent agreement with the empirical correlation of Figure 9.

The ratio of the computed average diametral-pressure gradient to the negative axial-pressure gradient $-\Delta P_D/\Delta P_\psi$ depends upon both the Dean number and the curvature ratio. Computed values, included in Table 2, ranged from 0.0105 to 6.5. At high Dean numbers and small curvature ratios, the diametral-pressure gradient can be quite significant.

Friction Factor

If the friction factor for curved-tube flow is defined in a manner similar to that for straight-pipe flow, it can be readily shown that the ratio of the friction factor for a curved pipe to that for a straight pipe is equal to the inverse of the ratio of the volumetric flux for a curved pipe to that for a straight pipe. The latter is given by the well-known Hagen-Poiseuille relationship. The volumetric flux for the toroid was calculated by integration of the computed axial-velocity profile over the flow cross section. The results are included in Table 2 and plotted in Figures 10 and 11. In Figure 10, the values are well grouped around White's experimental correlation (1929), and a slight

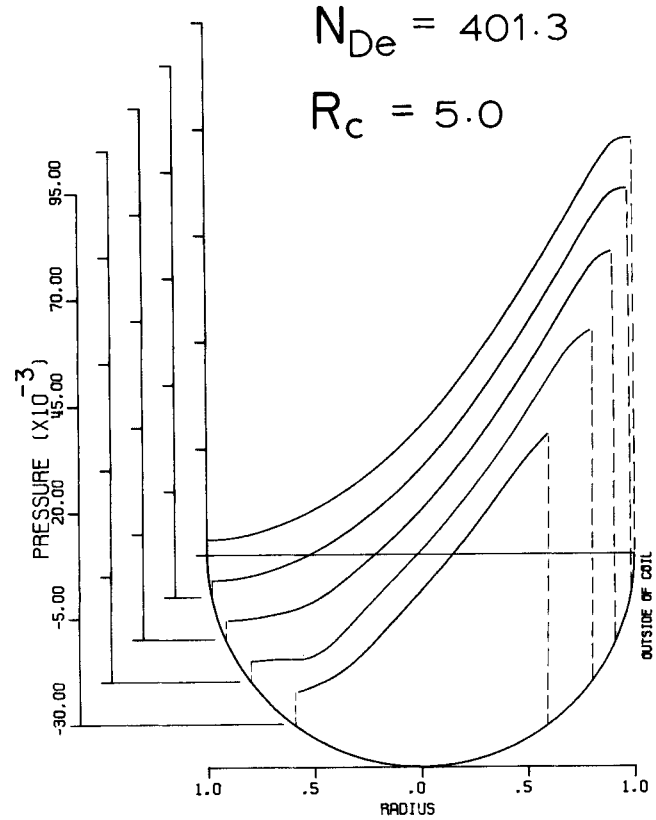

Fig. 8. Pressure distribution in secondary-flow plane.

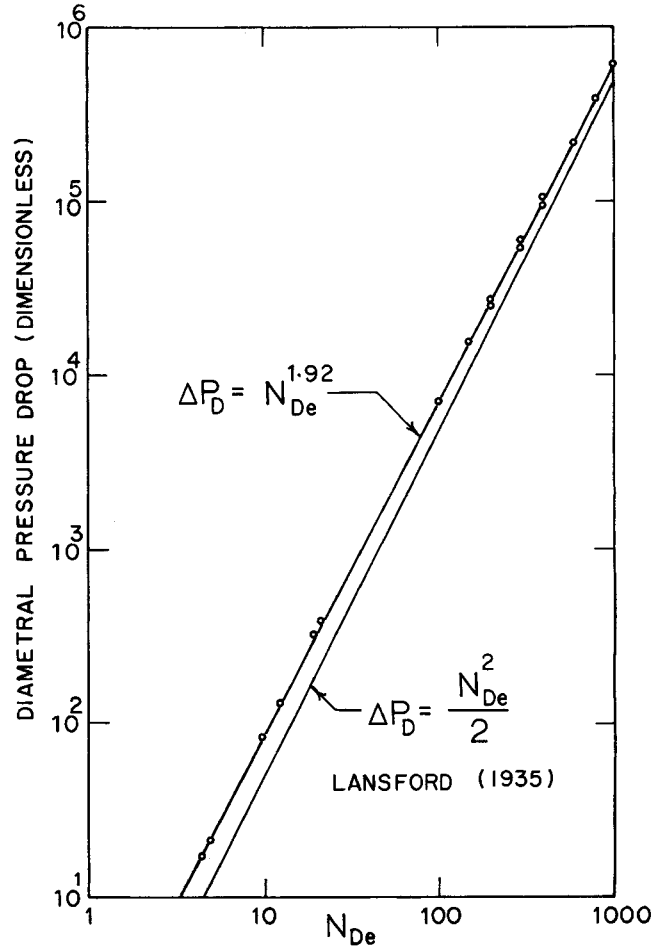

Fig. 9. Correlation of diametral-pressure difference.

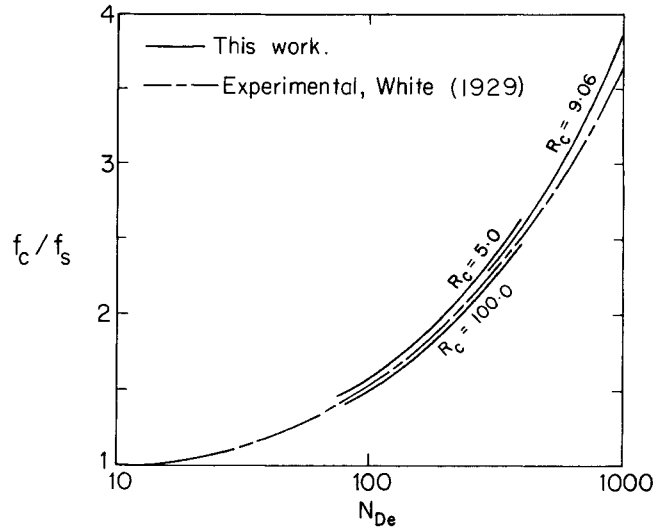

Fig. 10. Friction in curved tubes.

* The dimensionless form of the diametral pressure drop is based on the tube inside diameter. Therefore, ΔP_D may also be referred to as an average diametral pressure gradient.

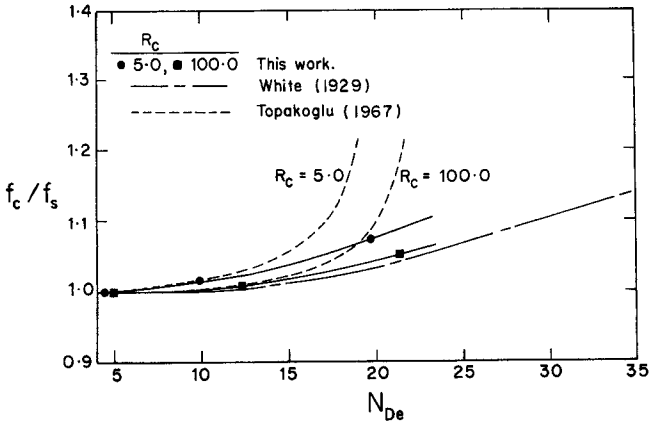

Fig. 11. Effect of curvature ratio on friction in curved tubes.

dependence on the curvature ratio can be noted. The analytical work of Topakoglu (1967) for low Dean numbers supports the validity of the curvature-ratio dependence, as shown in Figure 11. Topakoglu, extending Dean's original work but without simplifying the equations of motion, demonstrated a resistance law for toroidal flow that depended upon both the Dean number and the curvature ratio. As with Dean's, Topakoglu's solution was limited to low Dean numbers because of the difficulty of calculating additional coefficients in his expanded-series solution. The agreement of Topakoglu's solution with this work below a Dean number of approximately ten is noted in Figure 11.

A second method was used to compute the friction factor for curved-tube flow as a further check on the convergence of the numerical procedure. This method involved the computation of the peripheral distribution of point friction factors from the gradients at the wall of the axial components of the velocity. The velocity gradients were obtained by use of second- or third-order forward finite-difference expressions. Typical distributions are shown by Austin (1971). At high Dean numbers, the point friction factor increased dramatically in going from the inside of the coil to the outside of the coil. For example, at a Dean number of 400 and a curvature ratio of five, the overall increase corresponded to a factor of almost four. The peripheral distribution of the point friction factors was integrated to determine an average curved-tube friction factor. In general, friction factors computed in the second manner agreed with those computed from the first method to within one percent.

ACKNOWLEDGMENT

This research was supported primarily through a National Defense Education Act Fellowship in the Chemical Engineering Department at the University of Utah. Charles E. Kalb provided assistance in certain computations.

NOTATION

f_c = friction factor for curved tube, dimensionless
f_s = friction factor for straight tube, dimensionless
h = scale factor, dimensionless
N_{De} = Dean number $= N_{Re}(R/R_c)^{1/2}$
N_{Re} = Reynolds number $= 2R\rho\,\bar{v}_\psi/\mu$
p = combined static pressure and gravitational force in the form of a scalar potential, as defined in Bird et al. (1960), pp. 43-44
P = dimensionless pressure, defined by Equation (3)
r = radial coordinate in Figure 1
R = inside tube radius
R_c = radius of curvature
S = stream function, defined by Equations (12) and (13)
v = velocity vector
$\bar{v}$ = average velocity
V = dimensionless velocity, defined by Equation (2)

Greek Letters

ΔP_D = dimensionless average diametral-pressure gradient in the secondary-flow plane
$-\Delta P_D/\Delta P_\psi$ = ratio of diametral- to axial-pressure gradients
ΔP_ψ = dimensionless axial-pressure gradient $= (\partial P/\partial\psi)/R_c$
θ = angular coordinate in secondary-flow plane in Figure 1
μ = fluid viscosity
ν = fluid kinematic viscosity
ρ = fluid density
ψ = angular coordinate in axial direction in Figure 1
ω = vorticity

Subscripts

r = radial direction
θ = angular direction in secondary-flow plane
ψ = angular direction in axial direction

LITERATURE CITED

Akiyama, M., and K. C. Cheng, "Boundary Vorticity Method for Laminar Forced Convection Heat Transfer in Curved Pipes," *Intern. J. Heat Mass Transfer*, **14**, 1659 (1971).

Austin, L. R., "The Development of Viscous Flow Within Helical Coils," Ph.D. thesis, Univ. Utah (1971).

Bird, R. B., W. E. Stewart, and E. N. Lightfoot, *Transport Phenomena*, p. 119, Wiley, New York (1960).

Brodkey, R. S., *The Phenomena of Fluid Motions*, p. 60, Addison-Wesley, Reading, Mass. (1967).

Dean, W. R., "Note on the Motion of Fluid in a Curved Pipe," *Phil. Mag.*, **4**, 208 (1927).

Dean, W. R., "The Stream-Line Motion of Fluid in a Curved Pipe," *ibid.*, **5**, 673 (1928).

Eustice, J., "Flow of Water in Curved Pipes," *Proc. Roy Soc.*, **A84**, 107 (1910).

Eustice, J., "Experiments of Stream-Line Motion in Curved Pipes," *ibid.*, **A85**, 119 (1911).

Greenspan, D., *Introductory Numerical Analysis of Elliptic Boundary Value Problems*, Harper and Row, New York (1965).

Grindley, J. H., and A. H. Gibson, "On the Frictional Resistance to the Flow of Air Through a Pipe," *Proc. Roy Soc.*, **A80**, 114 (1908).

Ito, H., "Laminar Flow in Curved Pipes," *ZAMM*, **49**, 653 (1969).

Kalb, C. E., and J. D. Seader, "Heat and Mass Transfer Phenomena for Viscous Flow in Curved Circular Tubes," *Intern. J. Heat Mass Transfer*, **15**, 801 (1972).

Keulegan, G. H., and K. H. Beij, "Pressure Losses for Fluid Flow in Curved Pipes," *J. Res. Nat. Bur. Stand.*, **18**, 89 (1937).

Kubair, V., and N. R. Kuloor, "Secondary Flow in Helical Coils," *Indian J. Technol.*, **1**, 333 (1963).

Larrain, J., and C. F. Bonilla, "Theoretical Analysis of Pressure Drop in the Laminar Flow of Fluid in a Coiled Pipe," *Trans. Soc. Rheol.*, **14**, 135 (1970).

Lansford, W. M., discussion in *Trans. ASCE*, **100**, 1036 (1935).

Lapidus, L., *Digital Computation for Chemical Engineers*, McGraw-Hill, New York (1962).

McConalogue, D. J., and R. S. Srivastava, "Motion of a Fluid in a Curved Tube," *Proc. Roy. Soc.*, **A307**, 37 (1968).

Mori, Y., and W. Nakayama, "Study on Forced Convection Heat Transfer in Curved Pipes (1st Report, Laminar Region)," *Intern. J. Heat Mass Transfer*, **8**, 67 (1965).

Seban, R. A., and E. F. McLaughlin, "Heat Transfer in Tube Coils with Laminar and Turbulent Flow," *ibid.*, **6**, 387 (1963).

Schmidt, E. F., "Wärmeübergang und Druckverlust in Rohrschlangen," *Chem. Ing. Tech.*, **39**, 781 (1967).
Taylor, G. I., "The Criterion for Turbulence in Curved Pipes," *Proc. Roy. Soc. London*, **A124**, 243 (1929).
Topakoglu, H. C., "Steady Laminar Flows of an Incompressible Viscous Fluid in Curved Pipes," *J. Math. Mech.*, **16**, 1321 (1967).
Truesdell, L. C., Jr., and R. J. Adler, "Numerical Treatment of Fully Developed Laminar Flow in Helically Coiled Tubes," *AIChE J.*, **16**, 1010 (1970).
Truesdell, L. C., Jr., "Numerical Treatment of Laminar Flow Through Helical Conduits," Ph.D. thesis, Case Inst. Technol., Cleveland, Ohio (1963).
Vrentas, J. S., J. L. Duda, and K. G. Bargeron, "Effect of Axial Diffusion of Vorticity on Flow Development in Circular Conduits: Part I. Numerical Solutions," *AIChE J.*, **12**, 837 (1966).
White, C. M., "Stream-Line Flow Through Curved Pipes," *Proc. Roy. Soc.*, **A123**, 645 (1929).

Manuscript received January 5, 1972; revision received August 2, 1972; paper accepted August 7, 1972.

Effect of Mixing on Nonuniformly Initiated Polymerization by Radiation

An analytical study was carried out on the effects of mixing on radiation-induced polymerization in which the species initiating the polymerization were not uniformly produced because of a nonuniform dose rate distribution. The analysis is based on the periodic irradiation of fluid elements circulating in a stirred-tank reactor having a high dose rate region and a very low dose rate region. It is shown that the rate of polymerization increases with agitation speed and that the bimodal molecular weight distribution of the polymer formed at low agitation speed moves to a unimodal distribution as the agitation speed increases.

WAICHIRO KAWAKAMI and SUEO MACHI

Takasaki Radiation Chemistry Research Establishment
Japan Atomic Energy Research Institute
Takasaki 370-12, Japan

SCOPE

In this paper we present a simplified analytical method to predict the effect of mixing on radiation-induced polymerization in which the species initiating the polymerization were not uniformly produced because of a nonuniform dose rate distribution. Under the influence of the nonuniform dose rate distribution, the rate of active species formation is naturally nonuniform, and the efficiency of active species utilization in propagation reactions is low because of the high probability of their mutual deactivation in the high concentration.

The rate of radiation-induced chemical reaction usually has a dose rate exponent ranging from 0.5 to 1.0, depending on the deactivation mechanism of active species. In the case of reaction with dose rate exponent less than unity, it has been established that irradiation with a more uniform dose rate distribution gives a higher overall reaction rate for the same absorbed energy. If one can make the distribution of the active species more uniform by agitation before the deactivation, an increase in the reaction rate may be expected.

Up to this time, two different calculational methods have been reported. One is based on a diffusion model in which the radicals produced in the higher dose rate area are assumed to be dispersed throughout the reactor by diffusion (Noyes, 1959; Hill and Reiss, 1968). The other is based on a circulation flow model, in which fluid elements are assumed to be irradiated periodically by going around in the reactor (Fredrickson et al., 1961; Kawakami and Isbin, 1970).

CONCLUSIONS AND SIGNIFICANCE

The analysis is based on the periodoc irradiation of fluid elements circulating in a stirred tank reactor having a high dose rate region and very low dose rate region as shown in Figure 2. The practical consequences of the calculations are shown for the rate of polymerization and molecular weight distribution of polymer based on the polymerization of acrylamide in aqueous solution by an electron beam. It is shown that the rate of polymerization and number average molecular weight increase with agitation speed to attain values obtained under uniform irradiation by the average dose rate in the reactor. Also, the bimodal molecular weight distribution of the polymer formed at low agitation speed moves to a unimodal distribution as the agitation speed increases. If the energy absorbed in the reaction system is constant, there is a nonuniformity of dose rate distribution which gives a minimum polymerization rate.

The agitation speed required to attain perfect mixing